

Petrological evidence in support of the death mask model for Ediacaran soft-bodied preservation in South Australia

Tracking no: G45918R

Authors:

Alexander Liu (University of Cambridge), Sean McMahon (University of Edinburgh), Jack Matthews (Memorial University of Newfoundland), John Still (University of Aberdeen), and Alexander Brasier (University of Aberdeen)

Abstract:

Microbially mediated early diagenetic pyrite formation in the immediate vicinity of organic material has been the favoured mechanism by which to explain widespread preservation of soft-bodied organisms in late Ediacaran sedimentary successions, but an alternative rapid silicification model has been proposed for macrofossil preservation in sandstones of the Ediacara Member in South Australia. We here provide petrological evidence from Nilpena National Heritage Site and Ediacara Conservation Park to demonstrate the presence of grain-coating iron oxides, framboidal hematite, and clay minerals along Ediacara Member sandstone bedding planes, including fossil-bearing bed soles. SEM and petrographic data reveal that framboids and grain coatings, which we interpret as oxidized pyrite, formed before the precipitation of silica cements. In conjunction with geochemical and taphonomic considerations, our data suggest that anactuaistically high concentrations of silica need not be invoked to explain Ediacara Member fossil preservation: we conclude that the pyritic 'death mask' model remains compelling.

Petrological evidence in support of the death mask model for
Ediacaran soft-bodied preservation in South Australia

Alexander G. Liu¹, Sean McMahon², Jack J. Matthews^{3,4}, John W. Still⁵ and Alexander
T. Brasier⁵

¹ *Department of Earth Sciences, University of Cambridge, Cambridge, CB2 3EQ, U.K.*

² *UK Centre for Astrobiology, School of Physics and Astronomy, University of Edinburgh,
Edinburgh, EH9 3FD, U.K.*

³ *Department of Earth Sciences, Memorial University of Newfoundland, St. John's, NL A1C
3X5, Canada.*

⁴ *Oxford University Museum of Natural History, Oxford, OX1 3PW, U.K.*

⁵ *School of Geosciences, University of Aberdeen, King's College, Aberdeen, AB24 3UE, U.K.*

ABSTRACT

Microbially mediated early diagenetic pyrite formation in the immediate vicinity of organic material has been the favoured mechanism by which to explain widespread preservation of soft-bodied organisms in late Ediacaran sedimentary successions, but an alternative rapid silicification model has been proposed for macrofossil preservation in sandstones of the Ediacara Member in South Australia. We here provide petrological evidence from Nilpena National Heritage Site and Ediacara Conservation Park to demonstrate the presence of grain-coating iron oxides, framboidal hematite, and clay minerals along Ediacara Member sandstone bedding planes, including fossil-bearing bed soles. SEM and petrographic data reveal that framboids and grain coatings, which we interpret as oxidized pyrite, formed

before the precipitation of silica cements. In conjunction with geochemical and taphonomic considerations, our data suggest that an actualistically high concentrations of silica need not be invoked to explain Ediacara Member fossil preservation: we conclude that the pyritic ‘death mask’ model remains compelling.

INTRODUCTION

The taphonomy of the late Ediacaran Ediacara Member, South Australia—a silica-cemented, quartzofeldspathic arenite containing detailed three-dimensional moulds and casts of soft-bodied macro-organisms and matgrounds (e.g. Droser et al., 2017; Figure 1A)—has been the subject of considerable discussion. For almost 20 years, the leading explanation for the preservation of Ediacara Member macrofossils has been the ‘death mask’ model (Gehling, 1999), whereby extensive benthic microbial communities produced sulfides via sulfate reduction during burial, decay and early diagenesis. These sulfides are predicted to have reacted with iron in the sediment to form iron monosulfides and ultimately pyrite, rapidly mineralizing both the seafloor and the exterior impressions of any interred carcasses (Gehling, 1999). This mechanism is supported by petrological and sedimentological data from multiple late Ediacaran localities and facies (e.g. Gehling et al., 2005; Narbonne, 2005; Liu, 2016), although complementary processes such as clay mineral replication, kerogenization, adsorption of reduced iron onto organic matter, or pyritization contributed to preservation in some global settings (Laflamme et al., 2011; Schiffbauer et al., 2014; Ivantsov, 2016; MacGabhann et al., 2019).

Tarhan et al. (2016) proposed an alternative taphonomic model for the Ediacara Member, arguing that Ediacara-style exceptional preservation in sandstone, and the restriction of such preservation to the Proterozoic and early Palaeozoic, can be explained by the presence of

anactualistically high concentrations of marine dissolved silica. Ediacara Member silica cements within wave-base, sheet-flow and delta-front sandstone facies (the Oscillation-Rippled, Planar-Laminated and Rip-Up, and Flat-Laminated to Linguoid-Rippled Sandstone facies respectively of Tarhan et al., 2017) at Nilpena record Ge/Si ratios significantly higher than those of adjacent detrital sand grains, and so could not have derived their silica from these grains by metamorphic remobilization. The cements were instead interpreted to reflect preferential nucleation of silica directly from Ediacaran seawater onto microbial mats and organisms shortly after burial, welding the sand grains into coherent moulds that were stable enough to retain their relief throughout the collapse and decay of the carcasses. This model noted the paucity of clay or mud laminations between fossil-bearing part and counterpart surfaces (see Tarhan et al., 2017), and has been supported by uranium isotopic studies that interpret iron oxide veneers on fossil-bearing surfaces (considered a key line of evidence for original pyrite in the ‘death mask’ hypothesis; Gehling, 1999) to have been emplaced in the past two million years (Tarhan et al., 2018). Measured uranium isotope compositions ($^{234}\text{U}/^{238}\text{U}$) on these iron oxide-coated bed surfaces are far from secular equilibrium (Tarhan et al., 2018), leading those authors to conclude that the oxides were introduced into the sandstones during the Quaternary, precluding use of their presence or distributions as evidence to investigate original or early diagenetic conditions.

The ‘death mask’ and silicification hypotheses outlined above have distinct and important implications for our understanding of late Ediacaran marine biogeochemistry. The silicification hypothesis implies that silica was concentrated enough in the Ediacaran oceans to precipitate very near the seafloor in subtidal settings, despite known Ediacaran subtidal cherts generally being not primary but replacive after carbonate, and abundant subtidal cherts and silicilytes appearing only across the Ediacaran–Cambrian boundary (post-dating deposition of the Ediacara Member; Siever, 1992; Maliva et al., 2005; Brasier et al., 2011;

Perry and Lefticariu, 2014; Dong et al., 2015; Stolper et al., 2017). Conversely, the ‘death mask’ hypothesis implies that the decay and mineralization of widespread microbial matgrounds could have contributed to the high pyrite burial flux inferred for Ediacaran marine sediments (Liu, 2016; Shields, 2018). The taphonomic models also differ in their predictions regarding the interpretation of fossil morphology (Gibson et al., 2018). We here examine thin sections through South Australian fossil-bearing beds in an attempt to distinguish between these two competing models.

METHODS

We studied sedimentary samples representing nine distinct Ediacara Member fossil-bearing levels from Nilpena National Heritage Site (e.g. Figure 1B) and Greenwood Cliff in Ediacara Conservation Park, South Australia. Figured specimen AU15-2 originates from One Tree Hill, Nilpena, within the Oscillation-Rippled facies of the Ediacara Member (Droser et al., 2019). Figured specimens AU15-9 and AU15-12 come from North Ediacara Conservation Park close to Greenwood Cliff, in Flat-Laminated to Linguoid-Rippled Sandstone Facies (Coutts et al., 2016, following the terminology of Tarhan et al., 2017). Scanning electron microscopy (SEM) analysis of carbon-coated polished, uncovered thin sections cut perpendicular to bedding through fossil-bearing bed soles (Figure S1) was undertaken at the Aberdeen Centre for Electron Microscopy, Analysis and Characterisation facility at the University of Aberdeen using a Carl Zeiss GeminiSEM 300 VP equipped with Deben Centaurus CL detector, an Oxford Instruments NanoAnalysis Xmax80 EDS detector and Aztec Energy software suite. An accelerating voltage of 12 kV was used for CL imaging. Raman spectra were acquired with an inVia Raman system (Renishaw plc) coupled to a Leica DMLM microscope at the University of Edinburgh. The 785 nm excitation laser beam

(Toptica) was focused onto the samples using a $\times 100/0.9$ NA objective lens (Leica, HCX PL Fluotar), providing an excitation spot of 1 μm diameter. Raman point spectra were taken at different positions on the samples over the range 100–2000 cm^{-1} in extended scan mode. The spectra were acquired with 30 s exposure time using a 600 lines/mm diffraction grating and 8.8 mW excitation power. Wire 2.0 software was used for data acquisition.

RESULTS

Optical microscopy confirms the general character of the Ediacara Member fossil-bearing beds as quartzofeldspathic arenites bound by syntaxial silica cements in optical continuity with the host grains, as observed by Tarhan et al. (2016). However, widespread, abundant euhedral microcrystalline iron oxides are observed in direct contact with quartz and feldspar grains on fossil-bearing bed soles, and encased within the silica cement (Figures 2A–E, 3). SEM reveals that these iron oxides occur both at the present-day grain boundaries and as “ghosts” recording original sand grain boundaries, embedded fully within silica overgrowths (Figures 3E–F, S2). Iron oxides in these two settings are identical in appearance and contiguous in distribution (Figure S2C–D). We also identify laminae ≤ 1 mm thick, characterised by relatively fine sand-sized grains surrounded by abundant grain-coating iron oxides and clay mineral flakes, all within silica cement (Figures 2B, 2F, S3). The clay flakes are oriented plane-parallel to bedding, and commonly control the distribution of minor bedding-parallel fractures close to the bed soles. Such clay-rich laminae adhere directly to the hematite-rich bed sole in some samples (Figure S3). These laminae are extremely friable and easily lost during weathering, sampling, and sample preparation.

Associated with the iron oxide primary grain-coatings, and also present in small numbers in otherwise pure silica cements, we find discrete spherical structures $\sim 5\text{--}15$ μm in diameter.

These manifest as solid brown-red balls in transmitted light, but are revealed by SEM to comprise framboidal clusters of euhedral, submicron crystals identical to the grain coatings, and like them entirely encased within the silica cement (Figure 3). EDS reveals no evidence of sulfur (Figures S4, S5), and Raman spectroscopy confirms that the grain coatings and framboids are composed of hematite (Figure S6).

DISCUSSION

Our petrographic observations reveal horizons defined by hematite grain-coatings and clusters of hematite framboids within the fossil-bearing beds of the Ediacara Member. These iron oxides, located both at and within a few hundred microns of bed soles (Figure 3), are fully encased within the silica cements and must therefore pre-date silicification. Fossiliferous bed-soles themselves are hematite-rich (as recognised throughout the Ediacara Member, e.g. Figure 1A), and can be mantled by thin parting laminations characterised by abundant hematite grain-coatings and clay minerals (Figure S3). The silica-overgrown hematite “ghost” grain coatings are compositionally and morphologically identical to both the silica-cemented framboids and the hematite at younger grain boundaries. This implies that much (probably the majority) of the observed iron oxide originated as pyrite (though see Wilkin and Barnes, 1997, and references therein), which has subsequently been oxidised and preserved more or less *in situ* with limited redistribution. The iron- and clay-rich partings could also be interpreted as the weathering products of pyritic veneers (e.g. Gehling 1999). Taken together, our results are clearly compatible with Gehling’s (1999) ‘death mask’ model, bringing the Ediacara Member into line with other late Ediacaran fossil localities with evidence for both microbial surfaces and original pyrite and/or its oxidation products (Gehling et al., 2005; Liu, 2016). This global record, which appears to indicate early

diagenetic pyritization associated with microbially induced decay of organic matter in the absence of bioturbation, offers an anactualistic mechanism for the relatively high pyrite burial flux required by some Ediacaran biogeochemical models (e.g. Shields, 2018).

In addition to the petrological findings presented above, the silicification model faces further challenges that undermine its credibility as an explanation for Ediacaran taphonomic processes. First, Ediacara Member silica cements lack the disseminated carbon, clay and iron minerals that would be expected to have been trapped by the proposed nucleation of early-forming silica directly onto organic mats and carcasses. Such components are not readily lost from within impermeable amorphous/microcrystalline silica: they are pervasive in *bona fide* early-silica-cemented sandstone-hosted matgrounds as old as 3.2 Ga (e.g., Heubeck, 2009), as well as Precambrian and Early Palaeozoic cherts and silicilytes (including those cited by Tarhan et al., 2016). The absence of these components in the Ediacara Member silica cements indicates that any original silica cements have been lost, and that the observed cements were emplaced later.

Secondly, the Ge/Si ratios and petrographic observations central to the argument of Tarhan et al. (2016) may demonstrate that the Ediacara Member silica cements were extraneously sourced, but they do not necessarily indicate an early influx of silica from seawater. The relatively low Ge contents in detrital grains and high Ge contents in silica cements described by those authors are typical of ordinary Phanerozoic sandstones (Götte, 2016). The weak positive correlation between Al and Ge evident in the Ediacara Member cements (Tarhan et al., 2016; supp. table DR2) is also a familiar feature of Phanerozoic sandstone cements, likely resulting from the co-mobility of Al and Ge during diagenetic alteration of feldspar and/or kaolinite (Götte, 2016).

We also question the reasoning provided in previous dismissal of the ‘death mask’ model. Uranium data inferred to demonstrate a recent interaction between Ediacara Member facies and groundwater (Tarhan et al., 2018) do not establish that this interaction redistributed the iron oxides seen on bedding surfaces, or even that the uranium and iron oxide phases are specifically associated. Moreover, even supposing that the observed iron oxides did form within the last two million years, this finding would in no way undermine the original ‘death mask’ model, which allows for the late-stage oxidation of early diagenetic iron sulfides when exposed to groundwater. Given the burial and uplift history of Ediacaran sediments in South Australia, it is entirely feasible that the Ediacara Member was only oxidized within the past two million years. Observations of pristine framboidal pyrite veneers on fresh fossil-bearing Ediacaran surfaces in Newfoundland, Canada (Liu, 2016), alongside iron oxide staining with patchy surface distributions relating to modern groundwater flow, add weight to the suggestion that pyrite can remain unoxidized within Ediacaran-age sedimentary successions until modern exposure. The supposed improbability that iron sulfides could be produced rapidly enough to mould organisms prior to decay (Tarhan et al., 2016) requires experimental testing, and existing experimental data are encouraging (Darroch et al., 2012; Gibson et al., 2018). Similar concerns have been raised regarding whether microcrystalline quartz cementation would be capable of proceeding rapidly enough to act as the primary agent of macrofossil preservation (MacGabhann et al., 2019).

Definitive confirmation of the operation of the ‘death mask’ model in South Australia awaits the discovery of relict pyrite veneers clearly associated with individual macrofossil specimens. The small size of framboids necessitates undesirable destructive sampling of Ediacara fossils to investigate this. The few relevant studies that claim to bisect Australian Ediacaran fossil material (Retallack, 2016; SI of Tarhan et al., 2016) do not obviously provide images of mineralogy in the immediate vicinity of fossil specimens on bed bases.

Until such time as non-destructive microanalysis techniques of sufficient resolution are developed, conclusive demonstration of such thin pyrite veneers without damaging invaluable specimens will be challenging.

Our petrological investigation demonstrates the presence of clusters of hematite framboids, hematite cements directly coating sand grains, and clay minerals in Ediacara Member fossil-bearing sandstones, and indicates that the original iron-mineral cements and framboids pre-date silica cementation. The ‘death mask’ and silicification models are not necessarily mutually exclusive – determination of the absolute timing of silica cementation and sulfide formation would be required to conclusively disentangle them – but in light of our observations we consider the ‘death mask’ model to remain the most persuasive explanation for macrofossil preservation within the Ediacara Member.

ACKNOWLEDGEMENTS

Specimens were collected by AGL with permission and assistance from J. Gehling in 2015. AGL is funded by the Natural Environment Research Council [grant number NE/L011409/2]. SM acknowledges support from the European Union’s Horizon 2020 Research and Innovation Programme under Marie Skłodowska-Curie grant agreement 747877, and thanks M. Hall and A. McDonald for help with thin section polishing and Raman spectroscopy respectively. JJM recognises support from Mitacs, and all authors are grateful to N.J. Butterfield for constructive discussions during manuscript preparation. We thank R. Gaines, S. Darroch and J. Gehling for constructive reviews of this manuscript.

REFERENCES CITED

215 Brasier, M.D., Antcliffe, J.B., and Callow, R.H.T., 2011, Evolutionary trends in remarkable
 216 fossil preservation across the Ediacaran–Cambrian transition and the impact of
 217 metazoan mixing: Alison, P.J., and Bottjer, D.J. (Eds.), *Taphonomy*, Springer,
 218 Dordrecht, p. 519–567.

219 Coutts, F.J., Gehling, J.G., and García-Bellido, D.C., 2016, How diverse were early animal
 220 communities? An example from Ediacara Conservation Park, Flinders Ranges, South
 221 Australia: *Alcheringa*, v. 40, p. 407–421.

222 Darroch, S.A., Laflamme, M., Schiffbauer, J.D., and Briggs, D.E., 2012, Experimental
 223 formation of a microbial death mask: *PALAIOS*, v. 27, p. 293–303.

224 Dong, L., Shen, B., Lee, C.A., Shu, X., Peng, Y., Sun, Y., Tang, Z., Rong, H., Lang, X., Ma,
 225 H., Yang, F., and Guo, W., 2015, Germanium/silicon of the Ediacaran-Cambrian
 226 Laobao cherts: Implications for the bedded chert formation and paleoenvironment
 227 interpretations: *Geochem., Geophys., Geosyst.*, v. 16, p.751–763.

228 Droser, M.L., Tarhan, L.G., and Gehling, J.G., 2017, The rise of animals in a changing
 229 environment: global ecological innovation in the late Ediacaran: *Ann. Rev. Earth*
 230 *Planet. Sci.*, v. 45, p. 593–617.

231 Droser, M.L., Gehling, J.G., Tarhan, L.G., Evans, S.D., Hall, C.M.S., Hughes, I.V., Hughes,
 232 E.B., Dzaugis, M.E., Dzaugis, M.P., Dzaugis, P.W., and Rice, D., 2019, Piecing
 233 together the puzzle of the Ediacara Biota: Excavation and reconstruction at the Ediacara
 234 National Heritage site Nilpena (South Australia): *Palaeogeog., Palaeoclim., Palaeoecol.*
 235 v. 513, p. 132–145.

236 Gehling, J.G., 1999, Microbial mats in terminal Proterozoic siliciclastics; Ediacaran death
 237 masks: *PALAIOS*, v. 14, p. 40–57.

238 Gehling, J.G., and Droser, M.L., 2013, How well do fossil assemblages of the Ediacara Biota
 239 tell time?: *Geology*, v. 41, p. 447–450.

240 Gehling, J.G., Droser, M.L., Jensen, S.R., and Runnegar, B.N., 2005, Ediacara organisms:
 241 relating form to function: Briggs, D.E.G. (Ed.), *Evolving form and function: fossils and*
 242 *development*, Peabody Museum of Natural History, New Haven, p. 43–66.
 243 Gibson, B.M., Schiffbauer, J.D., and Darroch, S.A., 2018. Ediacaran-style decay experiments
 244 using mollusks and sea anemones: *PALAIOS*, v. 33, p. 185–203.
 245 Götte, T., 2016, Trace element composition of authigenic quartz in sandstones and its
 246 correlation with fluid–rock interaction during diagenesis: *Geol. Soc., London, Spec.*
 247 *Pub.*, v. 435, SP435-2.
 248 Heubeck, C., 2009. An early ecosystem of Archean tidal microbial mats (Moodies Group,
 249 South Africa, ca. 3.2 Ga): *Geology*, v. 37, p. 931–934.
 250 Ivantsov, A.Yu., 2016, Reconstruction of *Charniodiscus yorgensis* (macrobiota from the
 251 Vendian of the White Sea): *Paleontological Journal*, v. 50, p. 1–12.
 252 Laflamme, M., Schiffbauer, J.D., Narbonne, G.M., and Briggs, D.E.G., 2011, Microbial
 253 biofilms and the preservation of the Ediacara biota: *Lethaia*, v. 44, p. 203–213.
 254 Liu, A.G., 2016, Framboidal pyrite shroud confirms the ‘death mask’ model for moldic
 255 preservation of Ediacaran soft-bodied organisms: *PALAIOS*, v. 31, p. 259–274.
 256 MacGabhann, B.A., Schiffbauer, J.D., Hagadorn, J.W., Van Roy, P., Lynch, E.P., Morrison,
 257 L., and Murray, J., 2019, Resolution of the earliest metazoan record: Differential
 258 taphonomy of Ediacaran and Paleozoic fossil molds and casts: *Palaeogeography,*
 259 *Palaeoclimatology, Palaeoecology*, v. 513, p. 146–165.
 260 Maliva, R.G., Knoll, A.H., and Simonson, B.M., 2005, Secular change in the Precambrian
 261 silica cycle: insights from chert petrology: *GSA Bulletin*, v. 117, p. 835–845.
 262 Narbonne, G.M., 2005, The Ediacara biota: Neoproterozoic origin of animals and their
 263 ecosystems: *Annu. Rev. Earth Planet. Sci.*, v. 33, p. 421–442.

264 Perry Jr., E.C., and Lefticariu, L., 2014, Formation and geochemistry of Precambrian cherts:
 265 Treatise on Geochemistry, v. 7, p. 99–113.

266 Retallack, G.J., 2016, Ediacaran fossils in thin-section: *Alcheringa*, v. 40, p. 583–600.

267 Schiffbauer, J.D., Xiao, S., Cai, Y., Wallace, A.F., Hua, H., Hunter, J., Xu, H., Peng, Y., and
 268 Kaufman, A.J., 2014, A unifying model for Neoproterozoic-Palaeozoic exceptional
 269 fossil preservation through pyritization and carbonaceous compression: *Nature*
 270 Communications, v. 5, 5754.

271 Shields, G.A., 2018, Carbon and carbon isotope mass balance in the Neoproterozoic Earth
 272 system: *Emerging Topics in Life Sciences*, v. 2, p. 257–265.

273 Siever, R., 1992, The silica cycle in the Precambrian: *Geochimica et Cosmochimica Acta*, v.
 274 56, p. 3265–3272.

275 Stolper, D.A., Love, G.D., Bates, S., Lyons, T.W., Young, E., Sessions, A.L., and Grotzinger,
 276 J. P., 2017, Paleoecology and paleoceanography of the Athel silicilyte, Ediacaran–
 277 Cambrian boundary, Sultanate of Oman: *Geobiology*, v. 15, p. 401–426.

278 Tarhan, L.G., Hood, A. v.S., Droser, M.L., Gehling, J.G., and Briggs, D.E., 2016,
 279 Exceptional preservation of soft-bodied Ediacara Biota promoted by silica-rich oceans:
 280 *Geology*, v. 44, p. 951–954.

281 Tarhan, L.G., Droser, M.L., Gehling, J.G., and Dzaugis, M.P., 2017, Microbial mat
 282 sandwiches and other anactulistic sedimentary features of the Ediacara Member
 283 (Rawnsley Quartzite, South Australia): Implications for interpretation of the Ediacaran
 284 sedimentary record: *PALAIOS*, v. 32, p. 181–194.

285 Tarhan, L.G., Planavsky, N.J., Wang, X., Bellefroid, E.J., Droser, M.L., and Gehling, J.G.,
 286 2018, The late-stage “ferruginization” of the Ediacara Member (Rawnsley Quartzite,
 287 South Australia): Insights from uranium isotopes: *Geobiology*, v. 16, p. 35–48.

Wilkin, R.T., and Barnes, H.L., 1997, Formation processes of framboidal pyrite: *Geochimica et Cosmochimica Acta*, v. 6, p. 323–339.

FIGURE CAPTIONS

Figure 1. (A) The Ediacaran macrofossil *Dickinsonia costata* (SAM P51194) from the Ediacara Member of the Rawnsley Quartzite, Nilpena. (B) Field photograph of sedimentology within the wave-base (Oscillation Rippled) sand facies (*sensu* Gehling and Droser, 2013) at Nilpena.

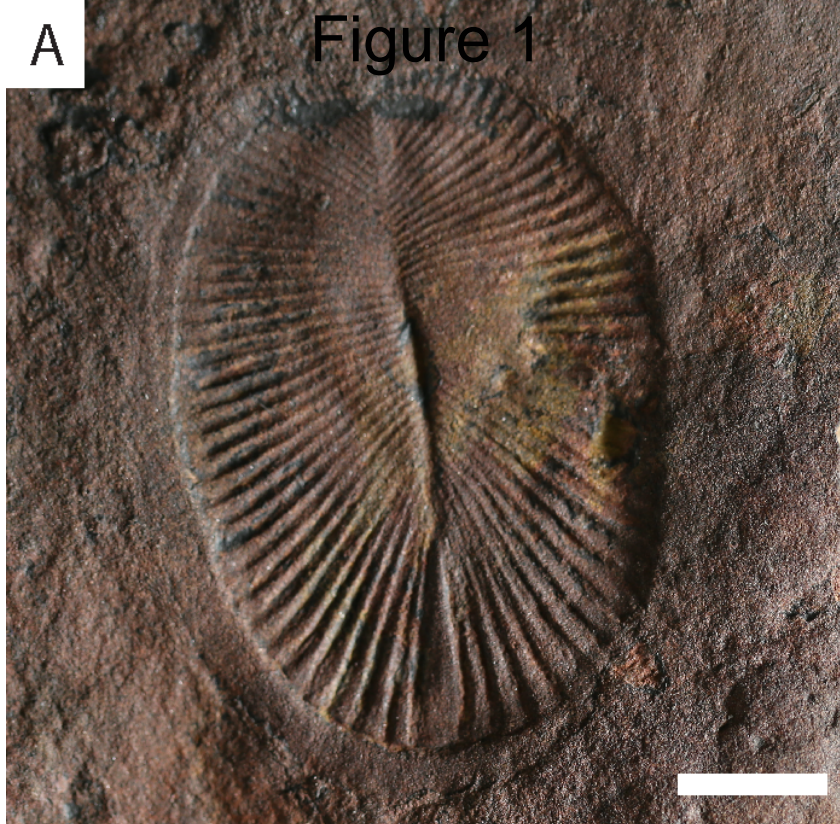
Figure 2. Thin section photomicrographs showing the distribution of framboidal structures and clay minerals in Ediacara Member sandstones. (A) Thin section AU15-9A in ppl, showing thin interbeds of coarse and fine sand, with several iron-oxide-rich horizons (arrowed). (B) Close up image of AU15-9A showing the abundance of clay minerals in the interstices between sand grains in the fine-grained laminae. (C) AU15-2 in ppl, showing a thin iron oxide veneer on a bed sole. (D) Close up of the region in the box in C), revealing the framboidal nature of the iron oxides, which appear to be resting on the upper surface of a quartz grain in a geopetal fashion and are encased in silica. (E) Reflected and transmitted light xpl view of AU15-9A, showing how red-brown hematite coats quartz grains along discrete horizons, with silica cement infilling the spaces after emplacement of the iron minerals. (F) Xpl view of AU15-12, with abundant clay mineral aggregates and detrital muscovite grains picked out by their high birefringence. Scale bars in A, C = 500µm; B = 200µm; D = 8µm; E–F = 80µm.

Figure 3. Scanning electron and transmitted-light (photo)micrographs showing framboidal microcrystalline iron oxide aggregates in thin section. (A) Photomicrographs of framboids in section AU15-12. The upper image was taken in plane-polarized light. The lower image, in cross-polarized light, shows that the silica cement surrounding the framboid is in optical continuity with the grain to the left. (B) Scanning electron micrograph of the boxed area in (A); framboid appears smaller because only crystals near the surface of the silica are visible. Scale bar = 5µm. (C) Photomicrograph showing multiple framboids on the surface of a quartz grain in sample AU15-2. Bed sole is at the top of the image. Scale bar = 8µm. (D) Scanning electron micrograph of sample AU15-12, showing framboid with euhedral crystals partly exposed by polishing. (E) Backscattered electron SEM image of a region at the bed sole of sample AU15-12, showing bands of Fe-oxides (white) seemingly in the middle of crystals. (F) Cathodoluminescence [CL] image of the same region in E), revealing that the Fe-oxides are located between two generations of quartz. Fe-oxides therefore coat original grains, and pre-date growth of the quartz cement. Scale bars (A–D) = 1 µm, (E–F) = 10 µm.

¹GSA Data Repository item 201Xxxx, [Specimen photographs, EDS and Raman data], is available online at www.geosociety.org/pubs/ft20XX.htm, or on request from editing@geosociety.org or Documents Secretary, GSA, P.O. Box 9140, Boulder, CO 80301, USA.

A

Figure 1



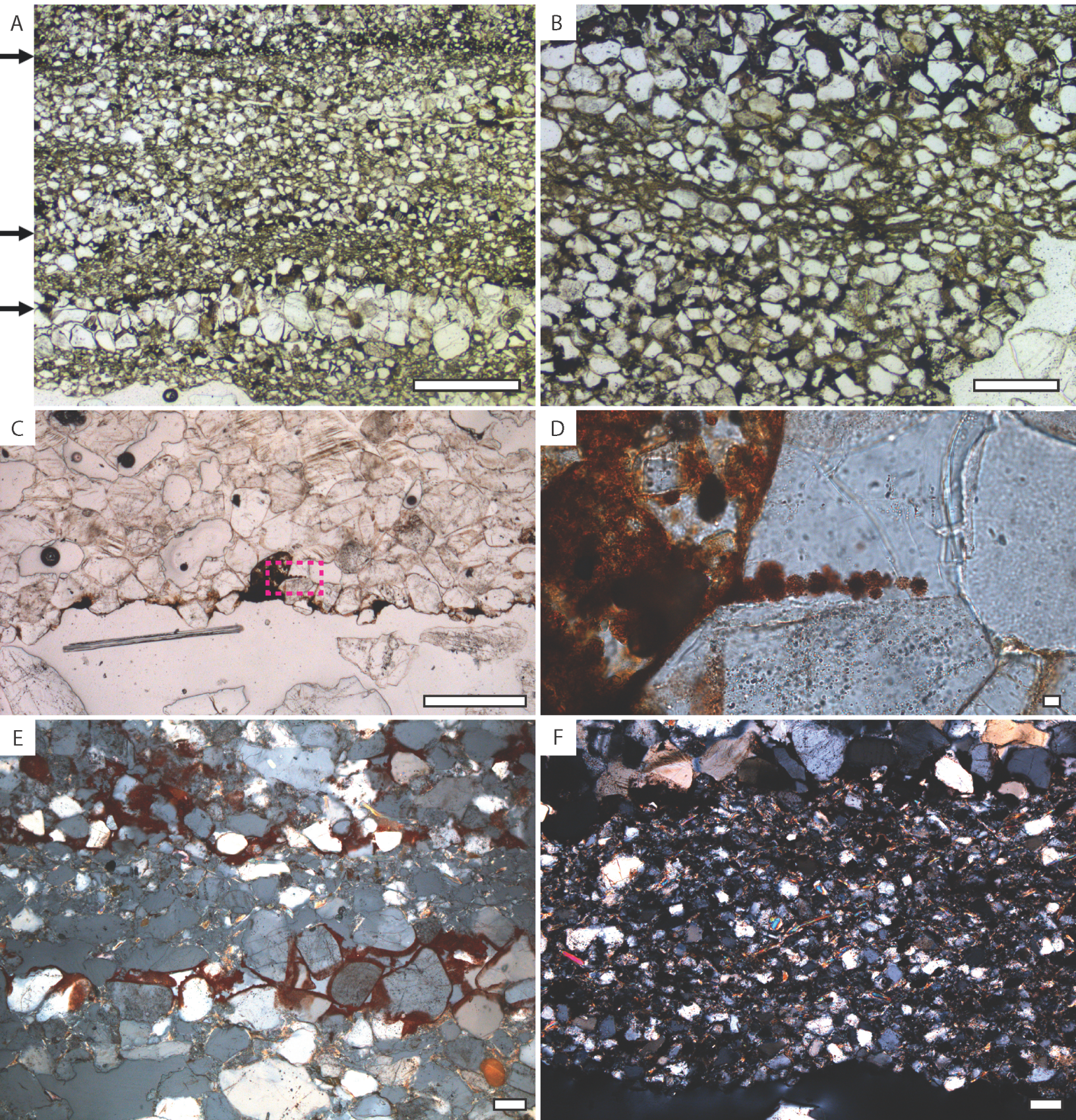
B



Liu et al, Fig. 1

Figure 2

Liu et al Fig. 2



Liu et al. Figure 3 Fig. 3

